Exponentially Tempered Lévy Sums in Random Lasers

Ravitej Uppu and Sushil Mujumdar*
Nano-optics and Mesoscopic Optics Laboratory, Tata Institute of Fundamental Research, 1, Homi Bhabha Road, Mumbai 400 005, India
(Received 21 June 2014; published 5 May 2015)

Lévy fluctuations have associated infinities due to diverging moments, a problem that is circumvented by putting restrictions on the magnitude of the fluctuations, realizing a process called the truncated Lévy flight. We show that a perfect manifestation of this exotic process occurs in coherent random lasers, and it turns out to be the single underlying explanation for the complete statistical behavior of nonresonant random lasers. A rigorous parameter estimation of the number of summand variables, the truncation parameter, and the power-law exponent is carried out over a wide range of randomness, inversion, and system size. Random laser intensity is modeled on a unique platform of exponentially tempered Lévy sums. The computed behavior exhibits an excellent agreement with the experimentally observed fluctuation behavior.

DOI: 10.1103/PhysRevLett.114.183903 PACS numbers: 42.55.Zz, 05.40.Fb, 42.25.Dd

Lévy fluctuations involving power-law decays $[P(x) \sim x^{-q}]$ are ubiquitously observed in the real world. Anomalous diffusion in disordered systems [1], trapping periods in the subrecoil cooling of atoms [2], foraging habits of marine predators [3], earthquake magnitudes [4], financial instruments [5], etc., exhibit power-law behavior of the related variables. In the optical domain, power-law decays have been reported in step lengths between scattering events in hot atomic vapors [6] and photon lifetimes in engineered disordered systems [7]. To such a medley of Lévy systems, random lasers [8–11] are a rather recent addition. Capable of both incoherent and coherent emission, these unique optical systems exploit disorder-enhanced amplification [12–22]. The innate disorder realizes statistical fluctuations in several systemic parameters [23–30], of which Lévy fluctuations of intensity, occurring in both dynamic [31–34] and static [35] disorder, have garnered particular interest. Lévy distributions have diverging moments, which generate the discussion on the paradox of "infinite variance in a real system" [36]. To resolve this paradox, two models have been proposed, namely, Lévy walks [37] and truncated Lévy flights [36]. The former involves spatiotemporal coupling, which penalizes extra-long displacements. The latter relies on the elimination of arbitrarily large jumps in variable values, effectively applying a truncation on the distribution. Such a truncation is justified by the physical limitations in any system. For example, natural systems such as earthquakes, forest fire areas, and even the fault lengths on Earth and Venus are studied using upper-truncated power laws, which yield more accurate system parameters [4].

The generalized central limit theorem (GCLT) states that the distribution of sums of Lévy variables $S_N = \sum_1^N x_i$, called Lévy sums, remains in the Lévy domain [38,39]. The introduction of a truncation forces the truncated Lévy sums to converge to a Gaussian process, thus precluding the diverging variance and resolving the infinity paradox [36]. Such a convergence is ultraslow, requiring a remarkably large number of summand variables. Therefore, reports on data from such systems remain limited to the applicability of a truncated power law. We find in our current studies that the coherent random laser based on nonresonant feedback qualifies as a physical system that inherently captures the convergence of a truncated Lévy sum to a Gaussian process. By investigating that range of disorder where the complete non-Gaussian and Gaussian behavior is observed, we show that the intensity statistics are completely described by a single platform of exponentially tempered Lévy sums. We obtain excellent agreement between the predicted behavior and our experimental observations.

In the nonresonant random laser, the distribution of intensity acquired by various spontaneously emitted photons is given by $P(I) \propto I^{-(1+\mu)}$, where $\mu = \ell_g/\langle L \rangle$, ℓ_g is the gain length, and $\langle L \rangle$ is the mean length of the photon paths [31]. Thus, the intensity acquired by a single photon path is a Lévy variable. However, it is not possible to access the intensities of the individual paths, as several of them coexist in the system and cannot be spatially or temporally separated for observation. Figure 1 schematizes the experimental measurement of the emission. Three representative photon paths are shown, whose emission frequency is assumed to be within the spectral resolution. Each path realizes a Lévy distributed intensity variable with exponent μ. All such paths are directed by a combination of a grating and a curved mirror inside the spectrometer onto the same pixel of the detector, which measures the total intensity summed over all paths. Thus, the measurement automatically sums the Lévy variables generated in the pulse. Furthermore, the finite energy of the excitation pulse limits the total gain in the random laser, which puts a truncation

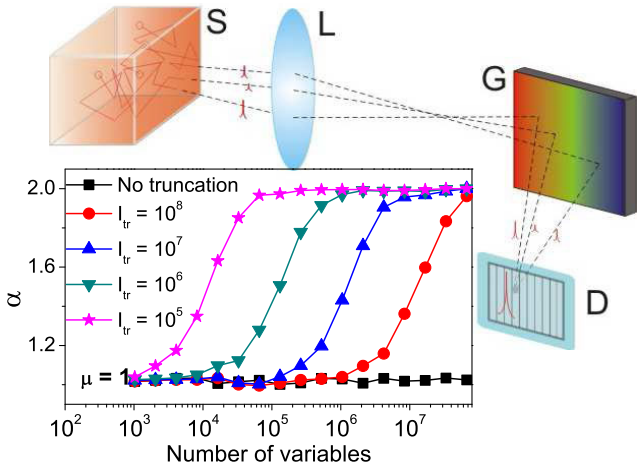

FIG. 1 (color online). Schematic of the summing process of Lévy variables in the experiment. Several photon paths at the same frequency are focused by a grating-curved mirror combination (here shown only as a grating G) onto the same pixel of the detector D, which measures them together. Plot: computed values of tail exponent α of the distribution of sums of truncated Lévy variables, which are distributed as a power law with $\mu = 1$. Black squares: no truncation. Finite truncation values result in α of the sum approaching 2, corresponding to the Gaussian domain.

on the individual intensities. Statistics are constructed out of the measured intensity values in thousands of such pulses. The statistical procedure utilizes an α-stable fit [33,34], which yields a tail parameter $0 < \alpha \leq 2$ (see Sec. I of the Supplemental Material [40]). α parametrizes the statistical distribution, since $\alpha < 2$ indicates Lévy behavior, and $\alpha = 2$ denotes Gaussian behavior. The plot in Fig. 1 elucidates calculated results on the effect of truncation on α of the distribution constructed by taking sums of power-law distributed random variables with exponent $\mu = 1$. The black squares represent an untruncated power-law distribution, wherein $\alpha = 1$ as expected from the GCLT. Subsequent finite truncation values of $I_{\mathrm{tr}} = 10^8$, 10^7, 10^6, and 10^5 result in $\alpha \to 2$. The crossover to the Gaussian domain requires the number of Lévy variables $N = A(I_{\mathrm{tr}})^{\mu}$, where A is a constant $\sim\mathcal{O}(1)$ [36]. Thus, the domain of random laser fluctuations will depend upon N, I_{tr}, and μ of the individual Lévy variables. We compute these parameters for various excitation energies, disorder strengths (parametrized by the mean free path ℓ), and sample sizes.

Accurate estimation of the Lévy variables requires the knowledge of exact photon paths and correct gain distributions. To that end, we analyzed the transport of light as random walks of photons in a three-dimensional random amplifying medium. This well-used computation has been described in complete details in Refs. [13] and [43]. In brief, the random walks of excitation photons first yield the realistic gain distribution in the medium. The excitation photons are launched from the front face, with a Gaussian transverse spatial distribution whose width emulated the pump laser focal spot. The sample space ($1 \times 1 \times 1$ cm) was divided into a 3D grid that recorded the population inversion with a resolution of $2 \times 2 \times 2$ μm. Subsequently, spontaneously emitted photons that underwent random walks in the inverted medium deexcited the system, realizing the random laser emission. Relevant parameters, such as the intensity, path length, wavelength, etc., of these exiting photons are recorded for subsequent analysis.

Figure 2 illustrates the simulation data and the parameter estimation for a sample with $\ell = 1500$ μm and the excitation energy $E_p = 1$ μJ. The inset shows the intensity distribution $P(I)$ of the scattered and the unscattered photons, exhibiting the expected power-law behavior. Parameter estimation is carried out using the survival function $[1 - F(I)]$, where $F(I)$ is the cumulative distribution function. The tail exhibits a smooth falloff, reflecting a gradual truncation. Such a behavior is indeed observed in real systems, where power-law infinities are tempered by an exponential smoothening [44,45]. We adopted a maximum likelihood estimate (MLE) method [46] to fit an exponentially tempered power law ($\sim x^{-\mu} e^{-\beta x}$) onto the data. (See Sec. II of the Supplemental Material [40].) The β parameter quantifies the truncation such that $1/\beta \sim I_{\mathrm{tr}}$, the value around which the exponential tempering begins. The red lines indicate the MLE fits, which cover the complete data including the falloff. The exponent $\mu = 0.52$ for the unscattered light was less than that of the multiply scattered light ($\mu = 0.68$) since the scattered photons navigate into the weakly pumped peripheral regions of the system, reducing the gain. Importantly, the unscattered component was strongly truncated ($I_{\mathrm{tr}} = 185$) compared to the scattered fraction ($I_{\mathrm{tr}} = 3 \times 10^4$). We consistently found small I_{tr} values for unscattered light for any excitation or disorder strength.

While the MLE fits provided μ and β of the exponentially tempered power-law distributions, the number of Lévy variables N_m was estimated as the number of photon paths

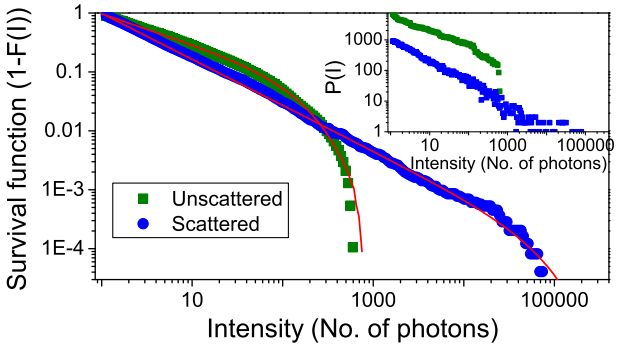

FIG. 2 (color online). Survival function of the unscattered (green squares) and scattered photons (blue circles), respectively. Red curves: estimated exponentially tempered power-law distribution using a maximum likelihood approach, giving exponents as 0.52 and 0.68 for unscattered and scattered photons. Inset: distribution of intensity showing the power-law decay.

incident on the detector, a parameter directly provided by the random walk computation. Thus, the parameter set $\{N_m, \mu, \beta\}$ was created for the scattered photons [47]. Here, we only illustrate results in the E_p and ℓ ranges where the rich statistical diversity is observed, although computations were carried out over a wider range of parameters. Figure 3 depicts the E_p dependence of the parameters for two disorder strengths, namely $\ell = 350$ μm (triangle markers) and $\ell = 1500$ μm (circle markers), and for small and large sample sizes, namely, pump focal diameter $d_p = 60$ μm (solid markers) and 240 μm (empty markers). Figure 3(a) shows the power-law exponent μ of the Lévy variables, which reduces monotonically with increasing E_p. For the small sample size, $\mu < 2$ indicating the Lévy distribution of the variables for all excitation energies. For weak disorder, μ is smaller since the excitation light propagates relatively unhindered in the medium, creating saturation. For the large sample size, we see that $\mu > 2$ for $E_p < 1.5$ μJ (indicated by a vertical dotted line), indicating Gaussian statistics due to insufficient gain. This domain, therefore, is not relevant for the convergence of the sums from a power-law to a Gaussian process. Figure 3(b) depicts the behavior of the truncation value $I_{\rm tr} = 1/\beta$, which consistently increases with pumping. The small sample exhibits large $I_{\rm tr}$ values ($\sim 10^8$ for $E_p \sim 2$ μJ), clearly realized by the stronger inversion. A larger truncation value implies the

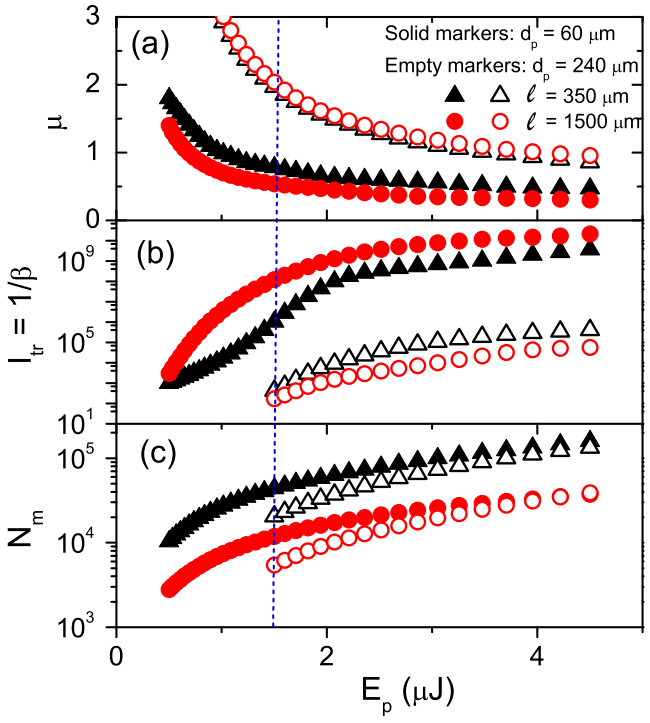

FIG. 3 (color online). Variation of the parameters of the ETLS, namely, (a) power-law exponent μ, (b) truncation value $I_{\rm tr} = 1/\beta$, (c) number of Lévy variables N_m with pump energy E_p as measured using the MLE method, for two ℓ and focal spot sizes d_p as mentioned in the legend.

allowance of larger magnitudes of the Lévy variables. For the larger sample, $I_{\rm tr}$ is reduced by about 4 orders of magnitude due to the distribution of pump energy over a larger volume. Interestingly, the magnitude of $I_{\rm tr}$ for the strong disorder is more than that for the weak disorder, a trend that is reversed as compared to the $d_p = 60$ μm sample. Figure 3(c) shows the variation of the number of Lévy variables N_m, which is seen to increase with E_p. For any given excitation, N_m is larger for smaller ℓ.

Subsequently, given μ and β for various combinations of ℓ, E_p, and d_p, exponentially tempered Lévy variables were generated by rejection sampling, as follows. (See also Sec. III of the Supplemental Material [40].) A power-law distributed random variable $y = u^{-1/\mu}$ is generated, where u is a uniform random number between 0 and 1. This y is accepted as an exponentially tempered power-law variable if, for another uniform random variable $v \in (0, 1]$, $f(y)/g(y) > v$, where $f(x) = x^{-\mu-1}e^{-\beta x}(\mu + x\beta)$ and $g(x) = \mu/(x^{\mu+1})$. Thereafter, using the appropriate N_m, a series of 2000 exponentially tempered Lévy sum (ETLS) values (S_N) was generated for each combination, such that $S_N = \sum_1^{N_m} y_i$. $P(S_N)$ was analyzed using the α-stable fit yielding the tail exponent α. The behavior of α characterized the simulated system over the complete parameter range. For immediate comparison with the experimental behavior, we carried out experiments on a dye-scatterer random laser, using suspensions of ZnO nanoparticles in a 2.5 mM rhodamine-methanol solution. The complete experimental setup is discussed in Sec. IV of the Supplemental Material [40]. A set of 2000 spectra was grabbed for analysis. The intensity values at $\lambda = 557$ nm were extracted from the spectra to create a distribution that was analyzed using the α-stable fit.

The calculated ETLS behavior and experimentally measured behavior of α is depicted in Fig. 4. Each image shows three subpanels, for the varying sample sizes in terms of focal spot size, namely, 60 μm (top), 120 μm (middle), and 240 μm (bottom). For the smallest sample size, in the weak disorder case ($\ell = 1500$ μm, the top row in the panel), a strong Lévy behavior is indicated by the blue pixels ($\alpha \sim 0.9$) at about E_p of 1 μJ. Here, the ETLS fails to converge to a Gaussian distribution, owing to the small N_m, small μ, and large $I_{\rm tr}$. Only for $E_p \geq 2.5$ μJ, the N_m suffices to drive the ETLS into a Gaussian distribution. In comparison, the Lévy behavior is seen to be very narrow for $\ell = 350$ μm. In this sample, for $E_p < 1.5$ μJ, although the individual variables are Lévy variables [$\mu < 2$ in Fig. 3(a)], the small $I_{\rm tr}$ in that region still forces a Gaussian behavior. The large variation in the widths of the Lévy domains across the disorder range also arises from the ETLS effect. For $d_p = 120$ μm, Lévy behavior is weak since the smallest $\alpha \sim 1.5$, and also the width of the Lévy region does not vary significantly. Interestingly, for the larger sample ($d_p = 240$ μm), a reversed trend is observed. Here,

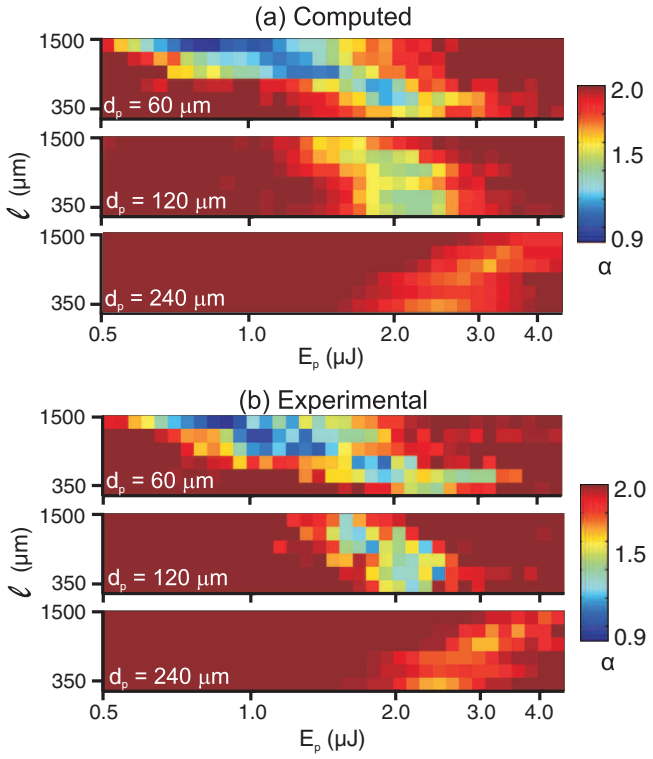

FIG. 4 (color). (a) Computed behavior of tail exponent α of the ETLS as a function of E_p and ℓ. Three images indicate focal spot size of 60 μm (top), 120 μm (middle), and 240 μm (bottom). (b) Experimentally measured behavior of α from a dye-scatterer random laser for the same parameters, showing an excellent agreement with the computed system.

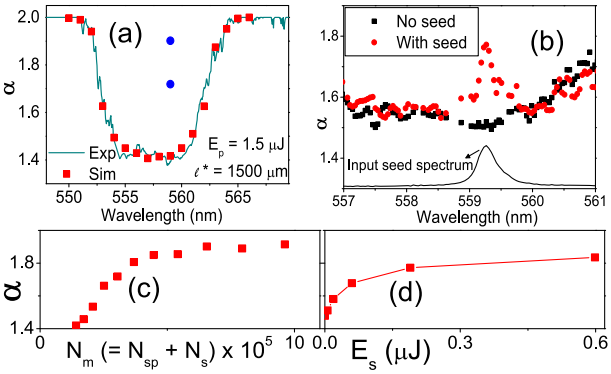

FIG. 5 (color online). (a) Wavelength dependence of α as seen in experiments (solid line) and the ETLS model computations (red ■'s). Blue circles show α when additional numbers of Lévy variables are assumed only at $\lambda = 559$ nm. (b) Experimental measurement of α after introducing additional Lévy variables by a seed pulse at $\lambda = 559$ nm. Seed spectrum is shown. (c) ETLS-computed variation of α with number of variables N_m where, N_m is a total of Lévy variables realized by spontaneous emission photons N_{sp} and seed photons N_s. (d) Experimental variation of α with seed energy E_s.

weak disorder requires a larger E_p ($\sim$3.4 μJ) to enter the Lévy domain as compared to the sample with $\ell = 350$ μm ($E_p \sim 2.4$ μJ). This originates from the larger I_{tr} for the latter sample [see Fig. 3(b)], which defeats the convergence of the ETLS into the Gaussian domain at a smaller E_p. For $\ell = 1500$ μm, conditions are appropriate for the Lévy domain only at $\sim$3.5 μJ. The experimental observations clearly show an excellent agreement with the predictions of the ETLS model. Features such as the widths of the Lévy domain, the magnitude of α, trends in the Lévy behavior, etc., are very well reproduced in the observations.

In a random laser, the relative fluctuations at the various wavelengths are not independent, as they are determined by the gain profile of the medium. To study the λ dependence of α, the parameter set $\{N_m, \mu, \beta\}$ was computed for a set of wavelengths using the same procedure described earlier. Thereafter, the ETLS constructed from these parameter sets yielded the behavior of α shown in Fig. 5(a) (red markers), which is in excellent agreement with the experimental data. This spectral dependence suggests a confirmatory test for the ETLS model. Since μ and β are inherently determined by E_p and ℓ, they cannot be independently tuned across the spectrum. On the other hand, N_m is determined by the number of photons that realize the Lévy variables, which can also be externally fed into the random laser. The ETLS model predicts that an increase in N_m, with μ and β constant, aids the convergence of the sum, thus raising α. In Fig. 5(a), the red square at $\lambda = 559$ nm involved $N_m = 1.4 \times 10^5$, while the lower and upper blue circles employed $N_m = 3 \times 10^5$ and 6.6×10^5, respectively. We used an external laser source that injected a certain number of seed photons into the random laser at a fixed wavelength, while keeping E_p and ℓ the same. We analyzed the α statistics of the output intensity at the seed wavelength. (See the Supplemental Material [40]) Figure 5(b) shows the α variation with (red markers) and without (black markers) the seed photons. Clearly, only the α's at the seed wavelength (over the seed bandwidth) increase in magnitude, obeying the spectral profile of the seed spectrum. Further, Fig. 5(c) shows the rise in α implemented by increasing N_m in the ETLS calculations. This expected behavior is clearly reproduced by the experimental observations, shown in Fig. 5(d), which plots α with seed energy E_s. These observations confirm the applicability of the ETLS model to the statistics of random lasers.

In summary, we have presented a physical manifestation of the stochastic process of exponentially tempered Lévy sums that determines the complete statistical behavior of nonresonant random lasers. The convergence of the Lévy sum, or the failure thereof, determines the ultimate statistical domain of the fluctuations. The theoretically expected behavior is in excellent agreement with the experimental observations. These studies provide a simple, yet powerful, handle to the nontrivial statistics of this complex optical system, and create a platform for further involved computational studies. We anticipate these results

to trigger the search for parallel scenarios in other research fields, as well as the study of the applicability of this stochastic process in other situations.

S. M. acknowledges helpful discussions with Azriel Genack, and financial support from the DAE, Government of India, towards Project No. XIIP0243: Optics of Random Nanomedia, and financial support from the DST through the Ramanujan Fellowship.

*mujumdar@tifr.res.in

[1] J.-P. Bouchaud, Phys. Rep., **195**, 127 (1990).
[2] F. Bardou, J.-P. Bouchaud, A. Aspect, and C. Cohen-Tannoudji, *Lévy Statistics and Laser Cooling: How Rare Events Bring Atoms to Rest* (Cambridge University Press, Cambridge, England, 2002).
[3] N. E. Humphries *et al.*, Nature (London) **465**, 1066 (2010).
[4] S. M. Burroughs and S. F. Tebbens, J. Pure and Appl. Geophys. **158**, 741 (2001).
[5] R. N. Mantegna and H. E. Stanley, *An Introduction to Econophysics: Correlations and Complexity in Finance* (Cambridge University Press, Cambridge, England, 2000).
[6] N. Mercadier, W. Guerin, M. Chevrollier, and R. Kaiser, Nat. Phys. **5**, 602 (2009).
[7] P. Barthelemy, J. Bertolotti, and D. S. Wiersma, Nature (London) **453**, 495 (2008).
[8] D. S. Wiersma, Nat. Phys. **4**, 359 (2008).
[9] H. Cao, J. Phys. A **38**, 10497 (2005).
[10] V. S. Letokhov, Zh. Eksp. Teor. Fiz. **53**, 1442 (1968) [Sov. Phys. JETP **26**, 835 (1968)].
[11] N. M. Lawandy, R. M. Balachandran, A. S. L. Gomes, and E. Sauvain, Nature (London) **368**, 436 (1994).
[12] H. Cao, Y. G. Zhao, S. T. Ho, E. W. Seelig, Q. H. Wang, and R. P. H. Chang, Phys. Rev. Lett. **82**, 2278 (1999).
[13] S. Mujumdar, M. Ricci, R. Torre, and D. S. Wiersma, Phys. Rev. Lett. **93**, 053903 (2004).
[14] M. Noginov, *Solid State Random Lasers*, Springer Series in Optical Sciences Vol. 105, (Springer, New York, 2005).
[15] C. Lopez, Nat. Phys. **4**, 755 (2008).
[16] C. Conti and A. Fratalocchi, Nat. Phys. **4**, 794 (2008).
[17] L. Leuzzi, C. Conti, V. Folli, L. Angelani, and G. Ruocco, Phys. Rev. Lett. **102**, 083901 (2009).
[18] N. Bachelard, S. Gigan, X. Noblin, and P. Sebbah, Nat. Phys. **10**, 426 (2014).
[19] C. Vanneste, P. Sebbah, and H. Cao, Phys. Rev. Lett. **98**, 143902 (2007).
[20] M. Leonetti, C. Conti, and C. Lopez, Nat. Photonics **5**, 615 (2011).
[21] J. Liu, P. D. Garcia, S. Ek, N. Gregersen, T. Suhr, M. Schubert, J. Mørk, S. Stobbe, and P. Lodahl, Nat. Nanotechnol. **9**, 285 (2014).
[22] P. Stano and P. Jacquod, Nat. Photonics **7**, 66 (2013).
[23] O. Zaitsev, Phys. Rev. A **74**, 063803 (2006).
[24] O. Zaitsev, Phys. Rev. A **76**, 043842 (2007).
[25] D. Anglos, A. Stassinopoulos, R. N. Das, G. Zacharakis, M. Psyllaki, R. Jakubiak, R. A. Vaia, E. P. Giannelis, and S. H. Anastasiadis, J. Opt. Soc. Am. B **21**, 208 (2004).
[26] S. Mujumdar, V. Türck, R. Torre, and D. S. Wiersma, Phys. Rev. A **76**, 033807 (2007).
[27] X. Wu and H. Cao, Phys. Rev. A **77**, 013832 (2008).
[28] R. Uppu and S. Mujumdar, Opt. Lett. **35**, 2831 (2010).
[29] A. K. Tiwari and S. Mujumdar, Phys. Rev. Lett. **111**, 233903 (2013).
[30] S. García-Revilla, J. Fernández, M. Barredo-Zuriarrain, L. D. Carlos, E. Pecoraro, I. Iparraguirre, J. Azkargorta, and R. Balda, Opt. Exp., **23**, 1456 (2015).
[31] S. Lepri, S. Cavalieri, G. -L. Oppo, and D. S. Wiersma, Phys. Rev. A **75**, 063820 (2007).
[32] E. Ignesti, F. Tommasi, L. Fini, S. Lepri, V. Radhalakshmi, D. S. Wiersma, and S. Cavalieri, Phys. Rev. A **88**, 033820 (2013).
[33] R. Uppu, A. K. Tiwari, and S. Mujumdar, Opt. Lett. **37**, 662 (2012).
[34] R. Uppu and S. Mujumdar, Phys. Rev. A **87**, 013822 (2013).
[35] G. Zhu, Lei Gu, and M. A. Noginov, Phys. Rev. A **85**, 043801 (2012).
[36] R. N. Mantegna and H. E. Stanley, Phys. Rev. Lett. **73**, 2946 (1994).
[37] M. F. Shlesinger, G . M. Zaslavsky, and J. Klafter, Nature (London) **363**, 31 (1993).
[38] P. Lévy, *Theorie de l'Addition des Variables Aleatoires* (Gauthier-Villars, Paris, 1954).
[39] B. V. Gnedenko and A. Kolmogorov, *Limit Distribution for Sums of Independent Random Variables* (Addison-Wesley, Cambridge, MA, 1954).
[40] See Supplemental Material at http://link.aps.org/supplemental/10.1103/PhysRevLett.114.183903, for the experimental details, which includes Refs. [41] and [42].
[41] R. Weron, Computationally intensive value at risk calculations, in *Handbook of Computational Statistics*, edited by J. E. Gentle, W. Härdle, and Y. Mori (Springer, Berlin, 2004). p. 911.
[42] I. A. Koutrouvelis, J. Am. Stat. Assoc. **75**, 918 (1980).
[43] S. Mujumdar, R. Torre, H. Ramachandran, and D. S. Wiersma, J. Nanophoton. **4**, 041550 (2010).
[44] J. Rosinski, Stoch. Proc. Appl. **117**, 677 (2007).
[45] M. M. Meerschaert, Y. Zhang, and B. Baeumer, Geophys. Res. Lett. **35**, L17403 (2008).
[46] M. M. Meerschaert, P. Roy, and Q. Shao, Comm. Stat. Theory and Methods **41**, 1839 (2012).
[47] The small I_{tr} for the unscattered photons always converged the distribution to a Gaussian distribution for all E_p and ℓ, and could not contribute to any asymptotic non-Gaussian behavior.